

PACS numbers: 42.55.Px; 42.60.Da; 42.60.Jf
DOI: 10.1070/QE2002v032n12ABEH002352

High-power single-transverse-mode ridge optical waveguide semiconductor lasers

V.V. Popovichev, E.I. Davydova, A.A. Marmalyuk, A.V. Simakov, M.B. Uspenskii, A.A. Chel'nyi, A.P. Bogatov, A.E. Drakin, S.A. Plisyuk, A.A. Sratonnikov

Abstract. **More than 200 mW of a single-transverse-mode cw output power is obtained from a semiconductor heterolaser by optimising the waveguide properties of its ridge structure. The laser-beam divergence is close to the diffraction limit and its brightness exceeds 5×10^7 W cm $^{-2}$ sr^{-1}. The calculated and experimental parameters of the laser beam are coincident with a high accuracy, which allows their reliable simulation.**

Keywords: *ridge laser, effective refractive index, diffraction-limited beam.*

1. Introduction

One of the remarkable ideas proposed by N.G. Basov and his co-workers was the use of a semiconductor as an active laser medium [1]. The fact that sales of semiconductor lasers in 2000 grew to represent 75 % of the global market for all lasers [2] shows to what extent this idea proved to be prophetic. This confirms in practice the unique properties of semiconductor lasers. For example, the total efficiency of some semiconductor lasers operating under standard conditions may exceed 50 %, which is only half as much as the efficiency of an ideal radiation source.

The growing applications of semiconductor lasers stimulate the continuous improvement of their parameters already over forty years due to the development of physics of semiconductors and quantum electronics.

In this paper, we report the results of our studies on the development of single-transverse-mode ridge lasers emitting in the red and near-IR ($\lambda \leqslant 1.5\,\mu$m) spectral regions. Lasers of this type clearly demonstrate how the solution of a modern physical problem leads to an important practical result – the development of a laser emitting a nearly diffraction-limited beam providing the output power density, which is close to that determined by the optical damage of the material.

V.V. Popovichev, E.I. Davydova, A.A. Marmalyuk, A.V. Simakov, M.B. Uspenskii, A.A. Chel'nyi M.F. Stel'makh Polyus Research and Development Institute, ul. Vvedenskogo 3, 117342 Moscow, Russia; **A.P. Bogatov, A.E. Drakin** P.N. Lebedev Physics Institute, Russian Academy of Sciences, Leninskii prosp. 53, 119991 Moscow, Russia; **S.A. Plisyuk, A.A. Sratonnikov** Moscow Institute of Physics and Technology (State University), Institutskii per. 9, 141700 Dolgoprudnyi, Moscow region, Russia

Received 4 October 2002
Kvantovaya Elektronika **32** (12) 1099 – 1104 (2002)
Translated by M.N. Sapozhnikov

2. Optical confinement of a beam in the horizontal direction in an active medium

It is well known that the transverse distribution of the field of an electromagnetic wave of semiconductor lasers is most often determined by an optical waveguide, i.e., its is specified by the transverse distribution of the permittivity of an active region. In a direction perpendicular to the structure layers (which is usually called the vertical direction) the optical waveguide is always determined by the layer structure, in which each layer has its own refractive index, all of them forming a quasi-planar waveguide. In the horizontal transverse direction, the situation can be more complicated. The optical confinement of a beam, or the optical waveguide, in the horizontal direction in lasers studied in this paper is provided by a ridge construction of the structure.

Fig. 1 shows the scheme and the SEM image of the output facet of a laser. Such a structure is prepared as follows. The upper layers of a planar heterostructure are subjected to profile etching only in the y direction, whereas no etching is performed in the z direction, so that the final structure has the form of a ridge of width W. No etching is performed within the ridge ($|y| < W/2$), all the layers located above the p-emitter are etched, and the p-emitter layer is partially etched. As a result, the ridge thickness h changes along the y axis from the initial thickness d_{em} of the emitter layer at $|y| > W/2$. Then, all the upper part of the structure, except the ridge surface, is covered or overgrown with an insulating layer. Finally, the entire surface is covered with a metal contact layer. Therefore, the upper electric contact of the structure is connected only with the ridge surface.

When the current flows through an electric channel restricted by the ridge width W, an optical inhomogeneity of the complex permittivity and of the refractive index of the active layer is produced in the direction of the y axis (due to a change in the gain and a change in the carrier concentration, respectively). This inhomogeneity can produce a waveguide in the structure, the so-called gain-induced waveguide (gainguide). However, it was shown in many studies that the waveguide properties of such a waveguide are insufficient for the formation of a stable field distribution in the y direction even at power densities of several milliwatts. For this reason, the main waveguide effect is produced in the horizontal direction in these lasers by the ridge shape itself by changing appropriately the residual thickness of h of the upper emitter layer in the y direction.

Let us analyse the waveguide properties of the structure

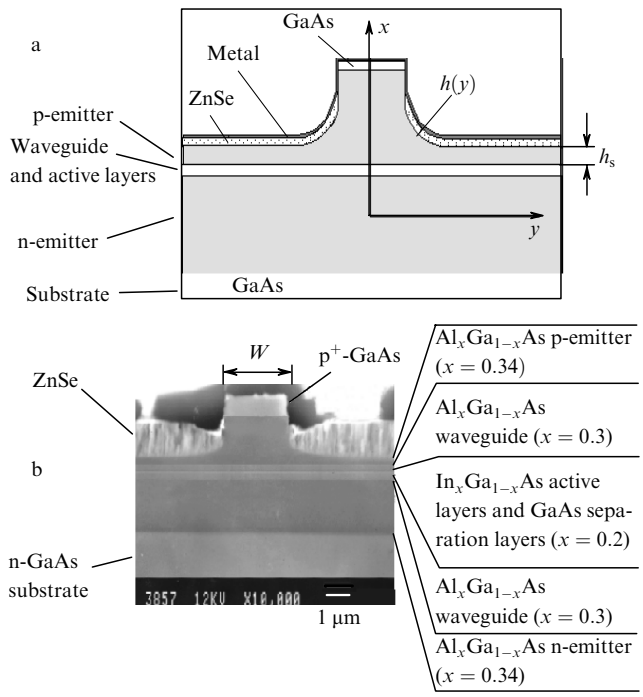

Figure 1. (a) Scheme and (b) photography of the output mirror of a ridge laser.

in the approximation of the effective refractive index, which was earlier developed and studied in many papers (see, for example, [3, 4] and references therein).

One can see from Fig. 1 that, due to formation of the ridge, the permittivity ε becomes a function of the transverse coordinates x and y even in the absence of pumping, i.e., in a 'cold' active region. The approximation is based on the fact that the spatial distribution of the field amplitude E in the laser can be represented in most practically interesting cases in the form

$$E = U(x,y)V(y)\exp(\mathrm{i}\beta z - \mathrm{i}\omega t), \tag{1}$$

where β is a complex constant of radiation propagation along the z axis and ω is the radiation frequency. The field amplitude E changes along the x axis much more rapidly than along the y axis, i.e.,

$$\left|\frac{\partial U}{\partial x}\right| \gg \left|\frac{\partial U}{\partial y}\right|, \quad \left|\frac{1}{U}\frac{\partial U}{\partial x}\right| \gg \left|\frac{1}{V}\frac{\partial V}{\partial y}\right|. \tag{2}$$

By substituting expression (1) for the field to the scalar wave equation and performing some elementary transformations, we obtain

$$\frac{1}{U}\frac{\partial^2 U}{\partial x^2} + \frac{1}{U}\frac{\partial^2 U}{\partial y^2} + 2\frac{1}{UV}\frac{\partial U}{\partial y}\frac{\partial V}{\partial y} + \frac{\omega^2}{c^2}\varepsilon(x,y) + \frac{1}{V}\frac{\partial^2 V}{\partial y^2} - \beta^2 = 0. \tag{3}$$

Because the two last terms are independent of x, being dependent only on y, we can denote this function as $\tilde{\beta}^2(y)$:

$$\tilde{\beta}^2(y) = \beta^2 - \frac{1}{V}\frac{\partial^2 V}{\partial y^2}. \tag{4}$$

Then, equation (3) can be written in the form

$$\frac{1}{U}\frac{\partial^2 U}{\partial x^2} + \frac{1}{U}\frac{\partial^2 U}{\partial y^2} + 2\frac{1}{UV}\frac{\partial U}{\partial y}\frac{\partial V}{\partial y} + \frac{\omega^2}{c^2}\varepsilon(x,y) - \tilde{\beta}^2(y) = 0. \tag{5}$$

By using relation (2), we can write equation (5) in the form

$$\frac{\partial^2 U}{\partial x^2} + \left[\frac{\omega^2}{c^2}\varepsilon(x,y) - \tilde{\beta}^2\right]U = 0. \tag{6}$$

The solution of equation (6) corresponds to the solution of a problem for a planar dielectric waveguide, whose permittivity is a function of one variable x, while y is a parameter of the problem. Therefore, by taking a fixed value y_0 and solving equation (6), we find simultaneously $U(x, y_0)$ and $\tilde{\beta}^2(y_0)$. By taking successively all the values of y_0, we find in this way the function $\tilde{\beta}^2(y)$. One can easily see that the function $\tilde{\beta}^2(y)$ represents the propagation constant of a wave in a planar dielectric waveguide. Therefore, it can be written in the form

$$\tilde{\beta}^2(y) = \frac{\omega^2}{c^2}\tilde{\varepsilon}_{\mathrm{eff}}(y) = \frac{\omega^2}{c^2}\tilde{n}^2_{\mathrm{eff}}(y), \tag{7}$$

where $\tilde{\varepsilon}_{\mathrm{eff}}(y)$ is the effective permittivity and $\tilde{n}_{\mathrm{eff}}$ is the effective refractive index. By substituting the found function $\tilde{\beta}^2(y)$ into (4), we obtain the equation

$$\frac{\partial^2 V}{\partial y^2} + \left[\frac{\omega^2}{c^2}\tilde{\varepsilon}_{\mathrm{eff}}(y) - \beta^2\right]V = 0, \tag{8}$$

which is analogous to (6). By solving this equation, we find finally the expression for the field (1), which contains the complex propagation constant β.

Therefore, the two-dimensional waveguide problem is solved successively as two one-dimensional problems by solving equations (6) and (8). We fix first the value $y = y_0$ for the permittivity and solve the problem for a waveguide, whose permittivity ε depends only on x: $\varepsilon(x) \equiv \varepsilon(x, y_0)$. The solution gives $\tilde{\beta}^2(y_0)$ or $\tilde{\varepsilon}_{\mathrm{eff}}(y_0)$ and $\tilde{n}_{\mathrm{eff}}(y_0)$. Then, the values $\tilde{\varepsilon}_{\mathrm{eff}}(y_0)$ or $\tilde{n}_{\mathrm{eff}}(y_0)$ found for different values of y_0 are already considered as functions of y, and the one-dimensional problem (8) is solved again, but already with some effective values of $\tilde{\varepsilon}_{\mathrm{eff}}(y)$ and $\tilde{n}_{\mathrm{eff}}(y_0)$. For this reason, this method is called the method of the effective refractive index.

Because the method of separation of variables was used earlier in the solution of the wave equation, as well as condition (2), of course, the well-known analogues of this method exist, for example, the Born – Oppenheimer approximation. The electron coordinate plays the role of the 'fast' coordinate x, while the nuclear coordinate y plays the role of the 'slow' coordinate. The main advantage of this method is its simplicity along with a comparatively satisfactory accuracy. Note here that conditions (2) are implicit because none of the functions $U(x, y)$ and $V(y)$ are initially known. Nevertheless, we can first solve the problem by assuming that conditions (2) are valid and then return to them to verify how adequate the obtained solution is. In addition, we can in principle refine the solution taking into account the dominant polarisation of radiation in solving equations (6) and (8).

Thus, the step function $\varepsilon(x, y_0)$ is specified by its values for all layers of the structure (Fig. 1) and by the thickness of these layers. Note that a certain thickness $h(y_0)$ of the p-emitter layer corresponds to a certain value y_0. By solving equation (6) for a set of thicknesses h, we will find $\tilde{n}_{\text{eff}}(h)$. Fig. 2 shows this dependence obtained for a quantum-well heterostructure used here. Then, using the measured etching profile $h(y)$ of the emitter layer, we find finally the transverse distribution of the effective refractive index $\tilde{n}_{\text{eff}}(y)$

$$\tilde{n}_{\text{eff}}(y) \equiv \tilde{n}_{\text{eff}}[h(y)]. \tag{9}$$

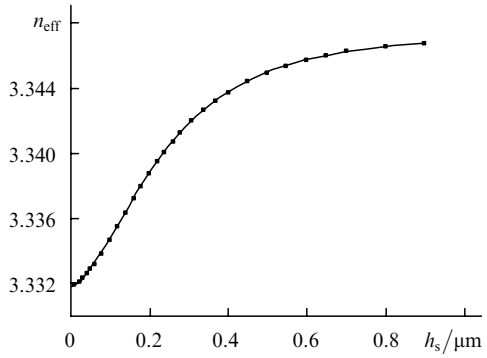

Figure 2. Dependence of the effective refraction index on the residual thickness h_s of a p-emitter layer.

Fig. 3 shows the horizontal profiles of the effective refractive index calculated, taking into account the data in Figs 1 and 2, for two ridge structures with different values of h_s. The profiles allow us to calculate the waveguide effect for the horizontal direction in the ridge semiconductor laser. Although Fig. 3 shows only the real part of $\tilde{n}_{\text{eff}}(y)$, it is obvious that, because the quantity $\varepsilon(x, y)$ is complex, the calculations give the complex values of $\tilde{\beta}^2(y)$ and $\tilde{n}_{\text{eff}}(y)$. For this reason, the effective horizontal profile of the complex permittivity $\tilde{\varepsilon}_{\text{eff}}(y)$ contains both the profile of the refractive index and the gain (absorption) profile.

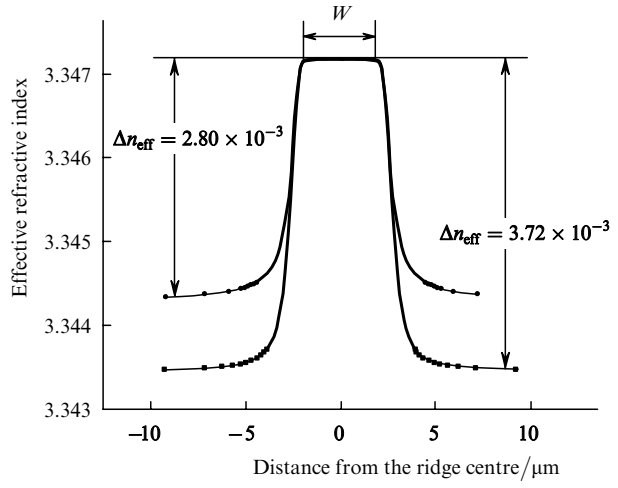

Figure 3. Calculated profile of the effective refractive index in the horizontal plane.

3. Optimisation of a waveguide to obtain a very bright laser beam

The studies have shown that, to obtain a high power in one transverse mode, the waveguide produced by the ridge structure should be optimised. This optimisation is the result of a balance of two opposite factors acting on lasing when the waveguide effect is changed. Thus, if the waveguide in the horizontal direction is weak, i.e., a jump in the effective refractive index is $\Delta\tilde{n}_{\text{eff}} \leqslant 10^{-3}$, then, although single-mode lasing is retained up to high powers, the field distribution itself is formed not only by a static waveguide built into the structure but also by a dynamic waveguide, which appears due to a temperature drop between the centre of the active region and remote passive (not pumped) regions. In addition, mechanical strains produced upon soldering of a laser diode can affect the spatial profile of the refractive index. Finally, one of the most undesirable effects of this type is the anti-waveguide action of injected carriers.

All these factors act on the waveguide effect approximately to the same extent and cause a jump in the effective refractive index $\Delta\tilde{n}_{\text{eff}} \sim 10^{-3}$. This leads to the instability in the horizontal distribution of the filed amplitude, which changes with the injection current of the laser, resulting in the nonlinearity of the watt–ampere characteristic, which is called a kink. To eliminate this undesirable effect, it is necessary to increase the efficiency of the built in waveguide by increasing a jump $\Delta\tilde{n}_{\text{eff}}$ in the effective refractive index.

It would seem that this can be achieved by etching a p-emitter layer more deeply in order to reduce its thickness h_s outside the ridge. However, when the value of $\Delta\tilde{n}_{\text{eff}}$ is increased considerably, for example, up to 10^{-2}, the waveguide can already sustain not only one fundamental mode but also higher-order modes. The lasing thresholds for all these modes approach each other with increasing $\Delta\tilde{n}_{\text{eff}}$. Fig. 4 shows the dependences of the threshold current for the first three modes on the thickness h_s, which were calculated using the data similar to those presented in Fig. 3. One can see that for $h_s \leqslant 0.37$ μm, lasing can occur both at the fundamental and the first mode, and for $h_s \leqslant 0.1$ μm, also at the second mode. Therefore, for the pump currents corresponding to the output power ~ 10 mW, lasing occurs at several transverse modes. Note that the distribution of a separated transverse mode in such a laser is very stable.

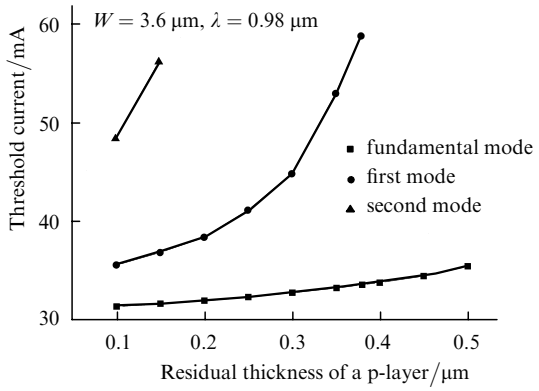

Figure 4. Dependences of threshold currents for the first three modes on the residual thickness h_s of a p-emitter layer.

Therefore, the design of a ridge laser is optimised, on the one hand, in order to create a horizontal waveguide with a sufficiently large $\Delta\tilde{n}_{\text{eff}}$, which provides a stable distribution of the fundamental-mode field, and, on the other hand, the value of $\Delta\tilde{n}_{\text{eff}}$ should be sufficiently small to avoid multimode lasing. The appropriate choice of $\Delta\tilde{n}_{\text{eff}}$ is very important for obtaining a high output power during lasing at one transverse mode. The necessity of such an optimisation of a horizontal waveguide was pointed out by Lang [5] as early as 1979. However, a laser with an optimal waveguide has been created only after extensive studies performed by many researchers, who proposed various technical solutions of the problem. Each of the stages of studies in this field was characterised by certain achievements. Here, we point out paper [6], in which one of the best results was obtained at present. In this respect, our paper also reflects a certain level, which has been obtained in the development of semiconductor lasers emitting diffraction-limited radiation. Below, we present the experimental results that characterise this level.

4. Experiment

We studied ridge lasers fabricated from quantum-well semiconductor $In_xGa_{1-x}As/Al_yGa_{1-y}As/GaAs$ heterostructures. The parameters of the layers of the laser structure and their refractive indices (and their corrected values given in parentheses) are presented in Table 1. The length of the resonator of laser diodes was 1000 μm, and the reflection coefficients of the output and rear mirrors were 3 % and 95 %, respectively. All the measurements were performed upon cw lasing at room temperature without cooling.

Table 1. Parameters of the layers of the laser structure under study.

Layer number	Layer	Layer composition x	Thickness/μm	Refractive index
1	p^+-GaAs	–	0.4	3.529
2	p-$Al_xGa_{1-x}As$	0.34 (0.349)	1.66	3.339 (3.334)
3	$Al_xGa_{1-x}As$	0.3 (0.295)	0.12	3.362 (3.365)
4	GaAs	–	0.007	3.529
5	$In_xGa_{1-x}As$	0.2	0.0053	3.60
6	GaAs	–	0.007	3.529
7	$In_xGa_{1-x}As$	0.2	0.0053	3.60
8	GaAs	–	0.007	3.529
9	$Al_xGa_{1-x}As$	0.3 (0.295)	0.12	3.362 (3.365)
10	n-$Al_xGa_{1-x}As$	0.34 (0.349)	3.0	3.339 (3.334)
11	n-GaAs	–	100	3.529

The far-field intensity distribution of laser radiation was detected with a computer-controlled setup described in paper [7]. The near-field intensity distribution of radiation at the output mirror was detected with a special optical setup containing a high-quality microobjective $0/\infty$ with a numerical aperture of 0.65 and a focal distance of 6.3 mm. The microobjective projected the output mirror of the laser diode on a CCD photodiode array (256 × 256 pixels), whose output signal was analysed with a PC. The required attenuation of radiation was achieved with the help of intermediate mirrors mounted between the objective and the CCD array. Glass plates without coatings with the reflection coefficient of 4 % – 5 % were used as such mirrors.

The setup provided the 260^x magnification of an object, so that 1 μm on the output mirror surface corresponded to 20 pixels of the CCD array. The output signals of the CCD matrix were analysed using a specially developed software, which represented the two-dimensional distribution of radiation in the CCD array plane as a product of one-dimensional distributions along coordinates x and y:

$$P(x, y) = S(x)F(y), \tag{10}$$

where $S(x) \simeq |U(x, 0)|^2$; $F(y) = |V(y)|^2$, which most adequately corresponds to the field representation according to expressions (1) and (2).

Fig. 5 shows the near- and far-field distributions of laser radiation for a 'fast' direction (along the x axis) perpendicular to structure layers (Fig. 1). Numerous measurements, performed in this paper and earlier, showed that these distributions are identical with high accuracy for all laser samples fabricated from the same batch. Moreover, these distributions are typically independent of the laser operation mode and characterise the heterostructure as a whole.

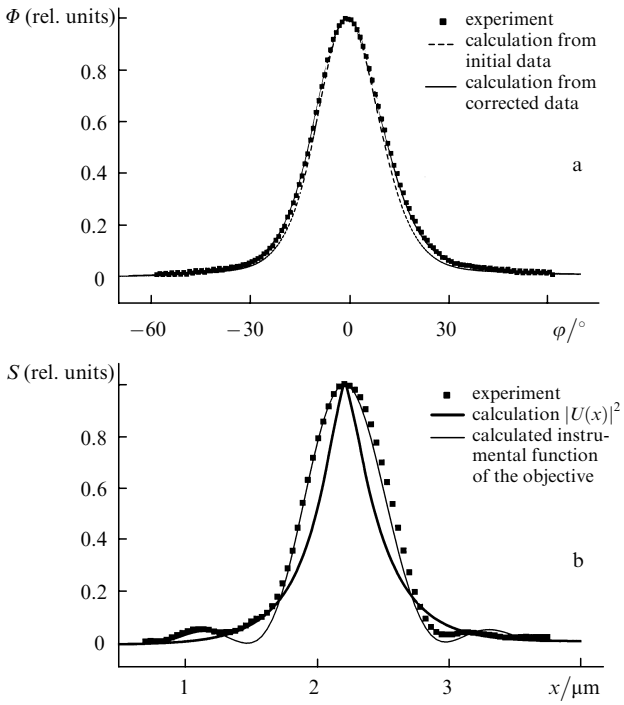

Figure 5. (a) Far-field $\Phi(\varphi)$ and (b) near-field $S(x)$ radiation intensity distributions in the vertical plane.

One can see from Fig. 5a that the radiation intensity distribution calculated from the parameters of layers used for the heterostructure fabrication is somewhat narrower (dashed curve) than the experimental distribution. By correcting the compositions within the accuracy of the structure fabrication (±2 %), we can achieve almost complete coincidence between the calculated and experimental far-field intensity distributions. Note that the size of squares corresponding to experimental data in Fig. 5a considerably exceeds the experimental error.

We calculated the far-field $\Phi(\varphi)$ and near-field $S(x) \sim |U(x, 0)|^2$ intensity distributions for the ridge centre ($y = 0$) by the method described in papers [8, 9]. Therefore, the measured far-field intensity distribution can be used to control the parameters of the grown heterostructure.

The near-field intensity distribution $S(x)$ in Fig. 5b has an almost trivial shape. The calculated distribution corresponding to the square of modulus $|U(x)|^2$ of the field amplitude of an eigenmode is somewhat narrower than the experimental distribution because of a finite spatial resolution of the setup, which is limited exclusively by the objective aberrations. This follows from good agreement between experimental data and the instrumental function of the objective calculated for the one-dimensional case and coherent illumination, which has the form

$$S(x) = \left[\frac{\sin(kAx)}{kAx}\right]^2, \tag{11}$$

where $k = 2\pi/\lambda$ is the wave vector in vacuum and A is the numerical aperture of the objective. Note that the one-dimensional condition is caused by a considerable ellipticity of a laser beam and corresponds to relations (2).

The radiation intensity distributions in the horizontal plane are no longer so unambiguous as in the vertical plane, as shown in Fig. 6. The calculation was performed for the profile $\tilde{\varepsilon}_{\text{eff}}(y)$, which was found by the method described in Section 2, taking into account a real geometry of the ridge structure (we used the dependence $h(y)$ in Fig. 1). The residual width of the p-emitter layer was $h_s = 0.45\,\mu\text{m}$ for the ridge width $W = 3.6\,\mu\text{m}$. The efficiency of a 'built in' waveguide produced by such a structure exhibits the jump $\Delta\tilde{n}_{\text{eff}} \approx 3 \times 10^{-3}$. For low pump currents (35–40 mA) corresponding to a small excess over the lasing threshold, the experimental and calculated distributions almost coincide, although the experimental distribution $F(y)$ is somewhat narrower than the calculated one. However, this difference is within the measurement error. The discrepancy between the experimental and calculated distributions somewhat increases with increasing pump current. The width of the experimental near-field intensity distribution decreases compared to the corresponding calculated width, whereas the experimental width of the far-field intensity distribution increases compared to the calculated width. Such behaviour can be explained by a weak dynamic change in the waveguide properties of the structure against the background of its strong 'built in' static waveguide. Because the spatial profile of the concentration of carriers along the y axis changes due to their inhomogeneous 'burning', the anti-waveguide property of carriers depends on the laser power and the pump current, i.e., the waveguide dynamic effect is provided. The carriers are burnt out to a greater extent at the central part under the ridge (compared to periphery regions), resulting in an additional waveguide effect. The horizontal near-field distribution of the wave intensity narrows down, whereas the far-field distribution widens correspondingly with increasing a total radiation power. In a laser with a 'weak' waveguide effect in the active region, this results in the self-action of the field on its own distribution and in the appearance of the transverse instability of the field [5, 10–12] and the nonlinearity of the watt-ampere characteristic in the form of hysteresis regions. In our case, the waveguide properties of the structure are quite strong, and the influence of carriers on the waveguide properties of the active region is reduced only to a change in the near- and far-field distributions of laser radiation.

Because the relative change in the intensity distribution in the horizontal direction with increasing laser power is small, the quality of the laser beam remains rather high.

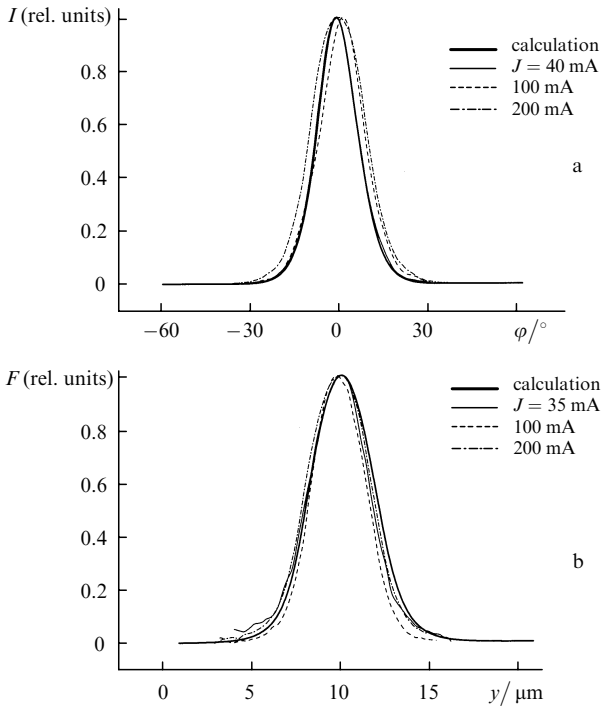

Figure 6. (a) Far-field and (b) near-field intensity distributions in the horizontal plane for different pump currents.

This can be verified by analysing the quantitative parameter M^2. In the case of the factorised representation of the transverse intensity distribution in a laser beam, this parameter can be written in the form

$$M^2 = M_x M_y, \tag{12}$$

where M_x and M_y are the factors for the vertical and horizontal planes, respectively. In our case, we can assume, with good accuracy, that $M_x = 1$. In the horizontal plane,

$$M_y = 2k\sigma_y\sigma_\varphi,$$

$$\sigma_y = \left[\frac{\int F(y)y^2\mathrm{d}y}{\int F(y)\mathrm{d}y}\right]^{1/2}, \tag{13}$$

$$\sigma_\varphi = \left[\frac{\int I(\varphi)\sin^2\varphi\mathrm{d}(\sin\varphi)}{\int I(\varphi)\mathrm{d}(\sin\varphi)}\right]^{1/2},$$

where σ_y and σ_φ are the mean-square sizes of the laser beam in the near- and far-field zones, respectively. For a Gaussian beam, the product $\sigma_y\sigma_\varphi$ is minimal and $M_y = 1$. The deviation of the beam divergence from the diffraction limit results in an increase in M^2. Expressions (13) were used for processing experimental near- and far-field intensity distributions.

Fig. 7 shows a typical watt–ampere characteristic of a laser with the optimised ridge structure. In this study, the laser output and the pump current were limited from above by the requirement of the laser reliability and the absence of the radiation damage of its output mirror. The initial part of the watt–ampere characteristic corresponds to $M^2 = 1$, i.e., to the diffraction quality of the laser beam. When the output power exceeded 100 mW, the factor M^2 increased some-

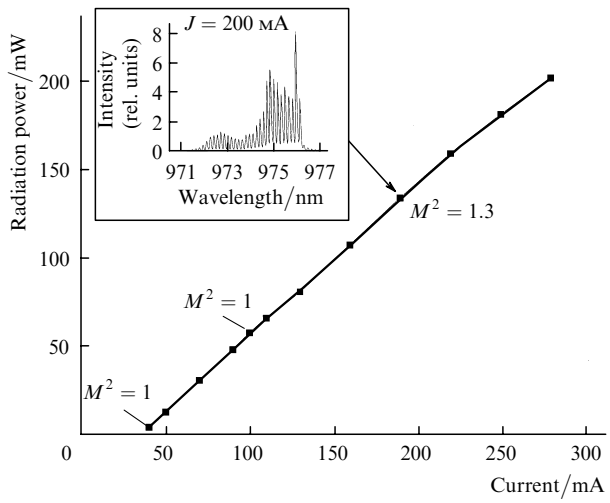

Figure 7. Typical watt–ampere characteristic of the optimised laser and the values of the quality parameter M^2 of the laser beam for different injection currents. The inset shows the emission spectrum of the laser for the pump current equal to 200 mA.

what, which was caused by the dynamic change in the intensity distribution; however, M^2 did not exceed, as a rule, 1.6 even for the output power ~ 200 mW.

We can estimate the angular brightness of the laser beam using the experimental data available. We will assume that the emitting area is limited by the radiation intensity at the 0.1 level of the maximum intensity. In this case, according to the data in Figs 5 and 6, the emitting area is estimated as $1.3\ \mu m \times 6.3\ \mu m \approx 8\ \mu m^2$, while the solid angle is estimated as 0.5 sr. Then, for the laser output of 200 mW, the average brightness of the laser is 5×10^7 W cm^{-2} sr^{-2}. The brightness is higher at the laser beam centre because we performed estimates by using not the half-widths of linear and angular sizes of the laser beam but substantially greater values.

The emission spectrum of studied lasers exhibited, as a rule, several excited longitudinal modes. A typical spectrum is shown in the inset in Fig. 7 for a current indicated by the arrow in the watt-ampere characteristic.

5. Conclusions

Having optimised the waveguide of a ridge laser, we obtained a single-transverse-mode output power of more than 200 mW, which was limited only by the laser reliability provided by the absence of radiation damage of the output facet. The quality of the laser beam was close to the diffraction limit. The output power can be increased by strengthening the output facet, which is a separate problem. It is possible that this will require a further improvement in the construction of the ridge laser.

Acknowledgements. The authors thank I.V. Akimova for her help in controlling the laser resonator geometry with the help of an electron microscope. This work was supported by the Federal scientific and technical programs 'Quantum and Nonlinear Processes' and 'Physics of Solid-State Nanostructures', the program 'Integration', the project 'Fundamental Optics of Quantum-Well Semiconductor Structures', and the INTAS Project No. 2001-571, and partially supported by Grant No. 00-15-96624 of the Leading Scientific Schools.

References

1. Basov N.G., Vul B.M., Popov Yu.M. *Zh. Eksp. Teor. Fiz.*, **37**, 587 (1959); Basov N.G., Krokhin O.N., Popov Yu.M. *Zh. Eksp. Teor. Fiz.*, **38**, 1879 (1960).
2. *Laser Focus World*, **2**, 85 (2001).
3. Evans G.A, Butler J.K., Masin V.S. *IEEE J. Quantum Electron.*, **24** (5), 737 (1988).
4. Buus J. *IEEE J. Quantum Electron.*, **18** (7), 1083 (1982).
5. Lang R. *IEEE J. Quantum Electron.*, **15** (8), 718 (1979).
6. Schmidt B., Pawlik S., Mauschek N., Miller J., Pliska T., Troger J., Lichtenstein N., Wittmann A., Moldriek S., Sverdlov B., Harder C. *Techn. Digest Opt. Fiber Comm. Conf. 2002* (2002, paper THGG64) p.702.
7. Bogatov A.P., Drakin A.E., Stratonnikov A.A., Konyaev V.P. *Kvantovaya Elektron.*, **30**, 401 (2000) [*Quantum Electron.*, **30**, 401 (2000)].
8. Stratonnikov A.A., Bogatov A.P., Drakin A.E., Kamenets F.F. *J. Opt. A: Pure Appl. Opt.*, **4**, 535 (2002).
9. Bogatov A.P., Drakin A.E., Luk'yanov S.A., Stratonnikov A.A., Ustinov A.V. *Kratk. Soobshch. Fiz. FIAN*, (8), 41 (1999).
10. Kirkby P.A., Goodwin A.R., Thompson G.H.B., Selway P.R. *IEEE J. Quantum Electron.*, **13**, 705 (1977).
11. Bogatov A.P., Eliseev P.G., Okhotnikov O.G., Pak G.T. *Kvantovaya Elektron.*, **5**, 2493 (1978) [*Sov. J. Quantum Electron.*, **8**, 1408 (1978)].
12. Bogatov A. *Proc. SPIE Int. Soc. Opt. Eng.*, **2399**, 456 (1995).